Published in final edited form as:
Pediatr Cardiol. 2012 August ; 33(6): 890–899. doi:10.1007/s00246-012-0249-0.

Structure/Function Relationship in the Sinus and Atrioventricular Nodes

Nikolaidou T[1,2], **Aslanidi OV**[3,4], **Zhang H**[4], and **Efimov IR**[1]

[1]Department of Biomedical Engineering, Washington University, St Louis, USA

[2]Faculty of Medical & Human Sciences, University of Manchester, Manchester, UK

[3]Department of Biomedical Engineering, King's College London, London, UK

[4]School of Physics & Astronomy, University of Manchester, Manchester, UK

Abstract

Recently published optical mapping studies in larger mammals, including human, have identified functionally discrete sino-atrial exit pathways of activation. This is in line with earlier mapping studies in dog and human but in contrast with findings in mouse and rabbit, where a propagation wavefront pattern of activation has been described. It underpins the complex 3D organization of the cardiac pacemaking and conduction system in larger species, where sinoatrial and atrioventricular nodal physiology both demonstrate identifiable activation pathways, which coincide with anatomical landmarks and histological architecture. So that, in addition to muscle fiber orientation and cell coupling, these intrinsic factors act to determine excitation pathways. This complex 3D organization increases the effect of source-to-sink mismatch both by greater variability of the space constant of tissue and by the 3D projection of this effect in all directions. Mathematical modeling provides a means to study these interactions and newer models should incorporate these additional factors and their effect in the 3D structure of large mammal physiology.

Keywords

Cardiac conduction system; Sinoatrial node; Atrioventricular node; Computer simulation

Introduction

The cardiac pacemaking and conduction system comprises the sinoatrial node (SAN), where electrical activation of the healthy atria begins, the atrioventricular node (AVN), responsible for channeling electrical conduction to the ventricles and serving as a backup pacemaker when the SAN fails, and the Purkinje network, which synchronizes ventricular activation. The cardiac pacemaking and conduction system exhibits automaticity i.e. consists of cells that develop spontaneous diastolic depolarization and pacemaking capacity [38]. This intrinsic pacemaking potential and its propagation to the myocardium is a complex process modulated by anatomical, physiological and humoral factors. Each component of this process can be studied individually, however, widespread efforts have been focusing on constructing mathematical models to predict the physiological behavior of cardiac excitation as a whole [16].

Corresponding author: Theodora Nikolaidou Room 360, Whitaker Hall, One Brookings Drive, Washington University, St Louis, Missouri MO 63130 nikolaidou@btinternet.com Phone: 314-935-6137 Fax: 314-935-7448.

Cardiac anatomy forms both bridges and barriers to electrical conduction. For example, the muscular Bachmann's bundle forms a direct inter-atrial connection [62], which facilitates synchronous activation of the atria [54]. Neurohumoral factors, such as the autonomic and renin-angiotensin systems, further act to modulate cardiac excitation through ionic channel and calcium handling regulation [25,28].

Conduction velocity is strongly dependent not only on fiber orientation [58] but also on intercellular coupling [55]. Tissues of the cardiac conduction system rely on cellular coupling to achieve two virtually opposing functions. Firstly, to reliably generate and conduct electric current to the overwhelming electrotonic load of the nearby myocardium; secondly, to remain electrotonically protected from the hyperpolarizing effects and arrhythmogenic currents in surrounding tissues. Smaller species have been studied more extensively in this respect, especially the mouse and rabbit, because of the technical experimental limitations in larger species. Ease of use of microelectrodes and possibility of genetic engineering in the rabbit and mouse SAN and AVN in contrast to larger mammals have been the two major reasons of focusing on small species.

The cellular architecture of nodal cells varies considerably from that of working myocardium. In the SAN, nodal cells are smaller, with fewer myofilaments and higher density of nuclei [8,39]. A gradient in myofilament content was found from center to periphery [48]. In the AVN, cells of varying sizes and myofilament content have been described [56,59]. The most accepted description of AVN cells relies on their action potential characteristics [7]. At the cellular level ion channel kinetics and gap-junction proteins modulate nodal excitability and coupling respectively. The “gradient model” was first introduced in SAN electrophysiology to describe the transitional properties exhibited by rabbit cells between the anatomically defined SAN and atrial tissue [14]. The same principle has been demonstrated by extracellular recordings exhibiting gradual changing properties across the AVN [21]. More recently, studies in the dog and human have described distinct SAN “exit pathways” [27,29].

The complexity of the cardiac conduction system further increases when the 3-dimensional (3D) arrangement of cells and fibers is taken into account and this degree of physiological complexity becomes harder to study, especially in larger species. Currents flow in and out of cells in multiple anisotropic directions, with the depolarized cells acting as the “source” of current, which diffuses into adjacent resting tissues (the “sink”). Such source-sink consideration is useful in determining the preferential direction of current (and hence, activation) spread in complex tissue architectures and the capacity of a relatively weak source of current within the SAN to drive the overwhelming electric load of the sink of well-coupled atrial myocardium. Quantitative differences between 2D and 3D cardiac fiber networks [45] or cardiac tissues models [6] are due to different source-sink relations. A 2D system with a point source needs to couple this source with a sink, which is proportional to λ^2, where λ is the space constant. In a 3D system, the sink is significantly larger, because it is proportional to λ^3. Thus, morphogenesis during development from a small heart with essentially a 2D pacemaker to an adult heart with a 3D pacemaker needs to match source-to-sink by significant anatomic and molecular engineering. The degree of complexity of this rearrangement becomes immediately apparent from a comparison between the 2D SAN of the mouse or rabbit heart and the 3D SAN of the canine or human heart.

Mathematical models with various degrees of biophysical detail have been developed for all major parts of the heart. The largest family of such models has been developed for rabbit, which includes models for the SAN and atria [4,18,46,68], ventricles and Purkinje fibers [6,12,61] and AVN [36,47]. These models incorporate large amount of electrophysiological and anatomical data. However, such data is not always well integrated: for example, families

of detailed electrophysiological models [6,36] were developed in parallel with the respective anatomical models [12,47]. Besides, results obtained from models of the rabbit heart, even when assembled from all available electrophysiological and anatomical data, are not necessarily translatable into studies of the human heart.

Using the same example as above, the thin quasi-2D structure of the SAN in rabbit [3] is different from the thick 3D structure of the SAN in human [19,25]. As a result, source-sink relationships between the SAN and the surrounding atria are different between rabbit and human. Therefore, the development of biophysically detailed 3D models based on human data is crucial for cardiac research. Although data from human cells and tissues is limited, several such models have been developed recently for the human SAN and atria [5,19] and are reviewed below.

The sinoatrial node

Structure

The sinoatrial node is the site of the primary cardiac pacemaker and is located in the inter-caval region of the right atrium, adjacent to the muscular crista terminalis (CT). Boineau et al. [10] described in humans using open chest mapping that the origin of the epicardial sinus impulse is anatomically varied and it can be multifocal, originating from more than one locations in the atria. In a dog model [11] two theories were proposed for atrial activation by the SAN: either separate pacemaker sites leading to different activation sequences or a single pacemaker site activating different sino-atrial pathways into the atria. The former organization was thought to be physiologically most favorable in small species with 2D SAN physiology, such as mouse and rabbit, while the latter organization was established in the larger 3D SANs of the canine [29] and human [27] hearts. Our recent studies in the canine and human SAN have demonstrated functional and structural properties of the sino-atrial exit pathways.

Inter-species variability has been noted not only in the precise location of the SAN but also in the thickness of the atrial wall that it occupies [14]. In general, the size of the SAN increases with larger species, as does the thickness of overlying endocardium and epicardium. For this reason extracellular recordings of the SAN are not technically feasible in larger species, unless the epicardium or endocardium are first stripped away [17]. The cycle length and action potential duration also increase with larger species [51].

Activation sequence and exit pathways

Small animal studies have shown that the leading pacemaker site can shift spontaneously and under different physiological and pathological conditions, such as autonomic stimulation and pharmacological intervention. In larger species such shift is evident as shift of the earliest breakthrough site at the epicardium or endocardium, due to utilization of different sino-atrial exit pathways [11,27,29,44,57]. This shift in the leading pacemaker and breakthrough sites is at least partly controlled by electrotonic influences from surrounding tissue. In small mammalian species investigators have demonstrated shift of the pacemaking site from the center to the periphery when the effect of atrial myocardium is removed [42] and this has been confirmed in a multicellular mathematical model [13]. Removal of the hyperpolarizing effect of atrial tissue unmasks the intrinsic faster spontaneous rate of the SAN periphery.

In small mammals, the activation sequence from the SAN has been described as a broad “wavefront” spreading towards the CT in a cranio-oblique course [28,65]. An area of conduction block, known as the “block zone” is located septally, preventing direct spread of the sinus impulse to the inter-atrial septum [24]. This zone of conduction block has been

identified in all species studied, including human [1,10,27–29,52]. Different hypotheses have been put forward, some attributing this area of conduction block to low excitability, as predicted mathematically [67]. However, the septal block zone was recently shown to consist of fibrous tissue with low numbers of myocytes in the rabbit [28] and an area of connective tissue, artery and fat in the human [27]. These findings make a physical electric barrier to conduction at this site more likely. In addition to this septal block, in larger mammals electric insulation is found in all directions, except for several sino-atrial exit pathways [27,29]. Conduction velocity was shown to slow down before exiting the SAN through these discrete pathways.

Experiments in animal preparations as well as a model of small balls of rabbit tissue [15,32] have demonstrated that SAN activation preferentially spreads along the axis parallel to the CT, as a result of favorable fiber orientation with a larger space constant in this direction [9]. Additionally, a gradient of increased refractoriness has been found from SAN periphery to center [41,43], which would not only contribute to protect the SAN but, in line with subsequent findings [53], may paradoxically increase the efficiency of conduction to the myocardium. This gradient of refractoriness has been attributed to ionic channel gradients [14] or a “mosaic” arrangement of atrial and SAN cells to explain this transition [60]. A simulation study suggested that the mosaic model may not account for the activation conduction pattern of an isolated SAN [66]. It is possible that in larger species, increased layers of connective tissue surrounding the SAN further add to this safety network.

Controversy surrounds the precise mechanism of atrial activation by the primary pacemaker. Boineau et al [11] attributed this to more than one “exit pathways” originating from more than one primary pacing sites. Conversely, in smaller species an activation “wavefront” has been described [28,30,65]. Bromberg et al [17] reported in the dog that SAN activation mapped with extracellular endocardial mapping did not follow the same pattern as that observed with intracellular microelectrodes. These discrepancies appear to reflect the different anatomical organization in large species, whereby the SAN is surrounded by layers of connective tissue separating it from the atrial cell layers, through which the sinus impulse needs to penetrate via the sino-atrial exit pathways and “breakthrough” to activate the atria. This concept of discrete pathways is supported by high-resolution optical mapping and histological studies in the dog [29] and human [27]. In the human SAN pacemaker shifts were recorded with atrial pacing. SAN activation originated from the anatomical SAN region in all cases but atrial conduction was initiated by at least three consistent exit pathways from SAN to atria (Fig. 1). These findings are in line with earlier in vivo studies in dog [11]. Additionally, there is evidence of increased connective tissue and presence of arterial branches at the conduction block zones. Biophysically detailed computational modeling of the human SAN [19], which, unlike experiments, enables in-depth access to the entire tissue, may help explain large mammal 3D physiology, by taking into account the 3D insulation of the SAN by connective tissue.

Mathematical models of the SAN

Several mathematical models have been developed to describe the complex pacemaking phenomena in the rabbit SAN [3,4,18,46,68]. These models incorporate extensive electrophysiological and anatomical data and are important in underpinning the mechanism of pacemaking in health and disease. An intrinsic limitation from the point of view of their application to clinical pacemaking problems lies in the inter-species differences between rabbit and mouse on one hand and human and canine on the other [27]. Primarily, the thin quasi-2D structure of the SAN in rabbit [22] is very different from the thick 3D structure of the SAN in human [27]. As a result, the source-sink relationship between the SAN and surrounding atria is different in larger species. Therefore, recently developed models of the human SAN and atria [5,19] are more suitable for addressing the problem of SAN activation

and exit pathways. The detailed 3D model of the human SAN by Chandler et al. [19] was based on a combination of imaging techniques—diffusion tensor MRI, histology, immunohistochemistry and image processing—and validated against available experimental data [10]. The model identified anatomical structures that may be responsible for the mechanisms of SAN activation and exit into the surrounding atrial tissue, including the orientation of myocytes and a “paranodal area” running alongside the SAN. This area is thought to possess properties of both nodal and atrial tissues and may have a role in pacemaking. Simulations of the model have shown that the paranodal area may depolarize the atrial overlay adjacent to the SAN and in this way facilitate exit of the action potential (AP) from the SAN into atrial muscle. The simulated SAN conduction time between the earliest excitation in the SAN and the earliest atrial activation (breakthrough) was ~120 ms (Fig. 2a), similar to that of ~70–100 ms observed experimentally in humans [27,40]. However, neither the model by Chandler et al. [19], nor a more detailed model of the entire 3D atria by Aslanidi et al. [5] demonstrated multiple well-defined breakthrough sites recorded by both electrode and optical mapping in canine and human hearts [11,27], because it did not incorporate the fibrous structure of the SAN surroundings (Fig 2b). Future mathematical models can be refined to incorporate the sino-atrial exit pathways as communication routes between the weak source of current within the SAN and the large 3D sink of the atrial myocardium. Furthermore, existence of a “paranodal area” needs to be confirmed by electrophysiological measurements in addition to histological data.

This model points to a possible explanation of the differences in results recorded from different species. Recording using thin SAN tissues from the rabbit [28] or mouse [30] may favor the continuous wavefront theory simply because the quasi-2D source-to-sink mismatch at the CT is proportional to λ^2 and is much weaker, conduction towards the CT is faster and the activation breaks through the surface evenly (almost isotropically) in the direction of the CT. The only source-sink matching required is the electrotonic uncoupling in the septal direction caused by a region of connective tissue. As the 3D structure in dog [26] and human [27] is much thicker, the source-to-sink mismatch is proportional to λ^3 and is stronger and thus has to be resolved by structural means. Such means include extension of a linear septal uncoupling of the SAN in 2D atria of the rabbit and mouse to a cylindrical uncoupling of the SAN from the atrial myocardium in the canine and human heart. This hypothesis can be tested by in-depth 3D mapping and modeling. It is also interesting to explore morphogenes that drive structural source-sink matching during cardiac development in such a different way in smaller and larger hearts with 2D and 3D SANs respectively.

Atrioventricular node

Structure

The AVN relays electrical activation from the atria to the ventricles in a tightly controlled manner. In addition, when sino-atrial activation fails, the AVN junctional pacemaker can take over cardiac excitation, serving as a backup pacemaker. It is located in the triangle of Koch, bound by the coronary sinus ostium at the apex, the septal leaflet of the tricuspid valve and the Tendon of Todaro [2]. This anatomical arrangement, similar to the SAN, creates discrete conduction pathways in the right atrium, through which electrical activation can reach the AVN (e.g. the thin septal isthmus between the coronary sinus ostium and the hinge of the tricuspid valve leaflet, which is the site of the “slow” pathway). The two predominant AVN pathways, the fast and slow pathways, consist of AVN extensions and nearby transitional atrio-nodal myocardium and occupy a tight space between working atrial myocardium and layers of fibrous tissue. This complex anatomical arrangement makes electrode recordings difficult. In the dog, AVN studies have required stripping of the endocardium for conducting microelectrode recordings [63]. In the human only optical mapping studies have been done so far [27,33].

Based primarily on electrophysiological characteristics of the rabbit AVN [7,21] cells have been classified as atrio-nodal (AN), nodal (N) and nodo-His (NH). This classification has been correlated with histological findings [23,47] as well as the discovery of “transitional” areas of intermediate protein expression both at the atrio-nodal junction and within the AVN itself in the rabbit [23,31,47,50]. In this way, AN cells are characteristic of the transitional area, nodal cells are typical of the compact node (CN) and NH cells make up the AV bundle. In contrast to the rabbit, larger species, including dog and human, are known to have at least two posterior extensions (rightward and leftward posterior extensions) [37]. More recently, the concept of “parallel longitudinal pathways” through the AVN has been developed in larger species based on Cx43 expression [34]. The rightward extension was shown to be in continuity with the lower nodal bundle and part of the His bundle in expressing significant Cx43 levels (presumed slow pathway), while the leftward extension and compact node had low Cx43 levels (presumed fast pathway). This indicates differential conduction pathways within the AVN, which could form the substrate of AV-nodal re-entry tachycardia. These findings have been strengthened by optical mapping studies, where more than one atrio-nodal pathways are discernible through the transitional zone [25,64] (Fig. 3). In the rabbit, the posterior nodal extension demonstrates low levels of Cx43, similar to the compact node [23].

Activation sequence and entry pathways

Following the source-sink approach the AVN presents a reversed situation, where electrical impulses from the atria need to be summated and funneled through a progressively diminishing area (sink). Although the situation is reversed, the AVN achieves this in similar ways to the SAN; firstly through a gradient of transitional tissue, secondly through the existence of more than one pathways into the AV node and, thirdly, by slowing of conduction and a long refractory period, which allows only controlled propagation to the ventricles [25,31,47,64]. In addition to this, it seems likely that the complex AVN anatomy reflects further points at which modulation of conduction can take place.

The “dual pathway” physiology to the AVN delineates the existence of two electrophysiological pathways, which can form re-entry circuits; one through the septal isthmus and a second through the atrial septum [49,50]. The precise anatomical and molecular substrate of these pathways is not fully described but the posterior nodal extension has been proposed as the site of the “slow pathway” in the rabbit [23] and dog [64]. In clinical electrophysiology, ablation of the slow pathway is known to terminate AV-nodal re-entry tachycardia. The human AVN has recently been studied in detail using optical mapping [25]. Fedorov et al. showed that in the human denervated heart the intrinsic junctional pacemaker is located in the nodo-His and His area, from where it shifts under autonomic control. When the AVN is paced from the right atrium there are two distinct antegrade atrio-nodal activation pathways (Fig. 3) but when junctional rhythm is allowed to propagate retrogradely multiple nodo-atrial exit pathways are seen.

Similar to the human, junctional activation in the dog originates in the nodo-His area [56]. This is in contrast to the rabbit, where junctional rhythm originates in the inferior nodal extension (INE) [23,35]. Also in the rabbit the junctional pacemaker is stationary under autonomic stimulation. [35]. Wu et al described three preferential antegrade pathways in the dog AVN [64]. In humans C×43 expression delineates two longitudinal pathways through the AVN (lower and upper pathways) [34]. The significance of this warrants further investigation. It seems to agree with earlier anatomical studies of the dog AVN [63]. The branching nature of fibers in the canine AVN led these investigators to the hypothesis of multiple non-linear pathways of conduction converging and diving again as they transverse the AV junction.

Mathematical models of the AVN

Numerous models for AVN conduction have been developed recently [20,36]. Climent et al. [20] suggested a phenomenological model for the activation time of the AVN. The model was validated against experimental data and accurately reproduced experimentally observed dual activation times through the fast and slow conduction pathways. However, this simple model did not consider details of electrophysiology and anatomy underlying the AVN conduction. A family of electrophysiologically detailed models for the AVN has been developed by Inada et al. [36], which included detailed AP models for single AN, N and NH cells. The models exhibited the same AP shapes and refractoriness as observed in experiments. Combining these models with models for the SAN and atrial muscle, Inada et al. also developed a one-dimensional (1D) multicellular model including both SAN and AVN. The multicellular model had slow and fast pathways into the AVN and was used to analyze the rich behavior of atrioventricular activation. Under normal conditions, APs were initiated in the SAN center and then propagated through the atrium and AVN. The relationship between the AVN conduction time and the timing of a premature stimulus (conduction curve) was also consistent with experimental data. After premature stimulation AVN re-entry could occur. During simulated atrial fibrillation the AVN was also shown to limit the number of APs transmitted to the ventricle, while in the absence of SAN pacemaking the INE acted as the pacemaker. Thus, the developed model [36] for the first time enabled detailed simulations of the typical physiological and pathophysiological characteristics of AVN conduction. The model can also be used in combination with the anatomically detailed model of the AVN developed by the same group [47].

Conclusions

This review aims to highlight the physiological complexity of the cardiac conduction system, which does not always allow direct observations to be drawn from anatomical studies alone. Paradoxical and counter-intuitive behaviors in this system make mathematical modeling an invaluable tool for creating hypotheses and predicting outcomes that could be tested experimentally.

Certain similarities can be drawn between activation of the SAN and AVN in the light of recent human studies. Firstly, both exhibit a shifting pacemaker physiology. Secondly, there are distinctly identifiable pathways connecting the SAN and AVN to the proximal atrial myocardium. It is likely that anatomical landmarks, such as the coronary sinus and location of the sinoatrial and atrioventricular nodal arteries, contribute to the establishment of these pathways. Fourthly, there is prominent electric insulation of the nodes from the nearby atrial myocardium by fibrous tissue. This insulation appears to facilitate safety of conduction between nodal and atrial tissues by matching two tissues with vastly different excitability and space constants. And lastly, both nodes exhibit significant inter-species differences, with clear distinctions between smaller and larger species, due to their 2D and 3D electrical architecture respectively. In the 3D larger mammalian SAN the source-sink mismatch is stronger and fibrous tissue needs to provide much more rigorous matching, as compared to the smaller mammalian 2D SAN. This can explain some of the discrepancies between published animal and human studies.

Optical mapping combined with 3D mathematical modeling can help clarify the fundamental methodological difference between 2D and 3D tissue organization. It will be interesting to investigate developmental aspects of this discrepancy, because the 2D pacemaker of the developing heart needs to undergo morphogenic reprogramming to become a safe pacemaker in a 3D SAN of the adult human. Exogenous factors, such as autonomic regulation, as well as human tissue genetic variability and the effect of remodeling by therapies, also need to be considered in the next generation of mathematical

models. In this review we have not discussed the Purkinje network physiology, which has attracted increasing interest and is likely to further improve our understanding of cardiac activation.

References

1. Alings AM, Abbas RF, de Jonge B, Bouman LN. Structure and function of the simian sinoatrial node (Macaca fascicularis). J Mol Cell Cardiol. 1990; 22(12):1453–1466. [PubMed: 2089159]
2. Anderson RH, Yanni J, Boyett MR, Chandler NJ, Dobrzynski H. The anatomy of the cardiac conduction system. Clin Anat. 2009; 22(1):99–113. doi:10.1002/ca.20700. [PubMed: 18773472]
3. Aslanidi O, Boyett M, Zhang H. Computer reconstruction of the cardiac pacemaker. Computers in Cardiology. 2006; (33):9–12.
4. Aslanidi OV, Boyett MR, Dobrzynski H, Li J, Zhang H. Mechanisms of transition from normal to reentrant electrical activity in a model of rabbit atrial tissue: interaction of tissue heterogeneity and anisotropy. Biophys J. 2009; 96(3):798–817. [PubMed: 19186122]
5. Aslanidi OV, Colman MA, Stott J, Dobrzynski H, Boyett MR, Holden AV, Zhang H. 3D virtual human atria: a computational platform for studying clinical atrial fibrillation. Prog Biophys Mol Biol. 2011; 107(1):156–168. [PubMed: 21762716]
6. Aslanidi OV, Stewart P, Boyett MR, Zhang H. Optimal velocity and safety of discontinuous conduction through the heterogeneous Purkinje-ventricular junction. Biophys J. 2009; 97(1):20–39. [PubMed: 19580741]
7. Billette J. Atrioventricular nodal activation during periodic premature stimulation of the atrium. Am J Physiol. 1987; 252(1 Pt 2):H163–177. [PubMed: 3812708]
8. Bleeker WK, Mackaay AJ, Masson-Pevet M, Bouman LN, Becker AE. Functional and morphological organization of the rabbit sinus node. Circ Res. 1980; 46(1):11–22. [PubMed: 7349910]
9. Bleeker WK, Mackaay AJ, Masson-Pevet M, Op't Hof T, Jongsma HJ, Bouman LN. Asymmetry of the sino-atrial conduction in the rabbit heart. J Mol Cell Cardiol. 1982; 14(11):633–643. [PubMed: 7154097]
10. Boineau JP, Canavan TE, Schuessler RB, Cain ME, Corr PB, Cox JL. Demonstration of a widely distributed atrial pacemaker complex in the human heart. Circulation. 1988; 77(6):1221–1237. [PubMed: 3370764]
11. Boineau JP, Schuessler RB, Mooney CR, Wylds AC, Miller CB, Hudson RD, Borremans JM, Brockus CW. Multicentric origin of the atrial depolarization wave: the pacemaker complex. Relation to dynamics of atrial conduction, P-wave changes and heart rate control. Circulation. 1978; 58(6):1036–1048. [PubMed: 709760]
12. Bordas R, Gillow K, Lou Q, Efimov IR, Gavaghan D, Kohl P, Grau V, Rodriguez B. Rabbit-specific ventricular model of cardiac electrophysiological function including specialized conduction system. Prog Biophys Mol Biol. 2011; 107(1):90–100. [PubMed: 21672547]
13. Boyett M, Holden AV, Kodama I, Suzuki R, Zhang H. Atrial modulation of sinoatrial pacemaker rate. Chaos, Solitons & Fractals. 1995; 5(3/4):425–438.
14. Boyett MR, Honjo H, Kodama I. The sinoatrial node, a heterogeneous pacemaker structure. Cardiovasc Res. 2000; 47(4):658–687. [PubMed: 10974216]
15. Boyett MR, Honjo H, Yamamoto M, Nikmaram MR, Niwa R, Kodama I. Downward gradient in action potential duration along conduction path in and around the sinoatrial node. Am J Physiol. 1999; 276(2 Pt 2):H686–698. [PubMed: 9950872]
16. Boyett MR, Li J, Inada S, Dobrzynski H, Schneider JE, Holden AV, Zhang H. Imaging the heart: computer 3-dimensional anatomic models of the heart. J Electrocardiol. 2005; 38(4 Suppl):113–120. [PubMed: 16226085]
17. Bromberg BI, Hand DE, Schuessler RB, Boineau JP. Primary negativity does not predict dominant pacemaker location: implications for sinoatrial conduction. Am J Physiol. 1995; 269(3 Pt 2):H877–887. [PubMed: 7573531]

18. Butters TD, Aslanidi OV, Inada S, Boyett MR, Hancox JC, Lei M, Zhang H. Mechanistic links between Na+ channel (SCN5A) mutations and impaired cardiac pacemaking in sick sinus syndrome. Circ Res. 2010; 107(1):126–137. [PubMed: 20448214]
19. Chandler N, Aslanidi O, Buckley D, Inada S, Birchall S, Atkinson A, Kirk D, Monfredi O, Molenaar P, Anderson R, Sharma V, Sigg D, Zhang H, Boyett M, Dobrzynski H. Computer three-dimensional anatomical reconstruction of the human sinus node and a novel paranodal area. Anat Rec (Hoboken). 2011; 294(6):970–979. [PubMed: 21538926]
20. Climent AM, Guillem MS, Zhang Y, Millet J, Mazgalev TN. Functional model of dual AV nodal pathway physiology. Conf Proc IEEE Eng Med Biol Soc. 2010; 2010:2646–2649. doi:10.1109/IEMBS.2010.5626539. [PubMed: 21096189]
21. de Carvalho A, de Almeida D. Spread of activity through the atrioventricular node. Circ Res. 1960; 8:801–809. [PubMed: 13808074]
22. Dobrzynski H, Li J, Tellez J, Greener ID, Nikolski VP, Wright SE, Parson SH, Jones SA, Lancaster MK, Yamamoto M, Honjo H, Takagishi Y, Kodama I, Efimov IR, Billeter R, Boyett MR. Computer three-dimensional reconstruction of the sinoatrial node. Circulation. 2005; 111(7): 846–854. [PubMed: 15699261]
23. Dobrzynski H, Nikolski VP, Sambelashvili AT, Greener ID, Yamamoto M, Boyett MR, Efimov IR. Site of origin and molecular substrate of atrioventricular junctional rhythm in the rabbit heart. Circ Res. 2003; 93(11):1102–1110. [PubMed: 14563715]
24. Efimov IR, Fahy GJ, Cheng Y, Van Wagoner DR, Tchou PJ, Mazgalev TN. High-resolution fluorescent imaging does not reveal a distinct atrioventricular nodal anterior input channel (fast pathway) in the rabbit heart during sinus rhythm. J Cardiovasc Electrophysiol. 1997; 8(3):295–306. [PubMed: 9083879]
25. Fedorov VV, Ambrosi CM, Kostecki G, Hucker WJ, Glukhov AV, Wuskell JP, Loew LM, Moazami N, Efimov IR. Anatomic localization and autonomic modulation of atrioventricular junctional rhythm in failing human hearts. Circ Arrhythm Electrophysiol. 2011; 4(4):515–525. [PubMed: 21646375]
26. Fedorov VV, Chang R, Glukhov AV, Kostecki G, Janks D, Schuessler RB, Efimov IR. Complex interactions between the sinoatrial node and atrium during reentrant arrhythmias in the canine heart. Circulation. 2010; 122(8):782–789. doi:10.1161/CIRCULATIONAHA.109.935288. [PubMed: 20697021]
27. Fedorov VV, Glukhov AV, Chang R, Kostecki G, Aferol H, Hucker WJ, Wuskell JP, Loew LM, Schuessler RB, Moazami N, Efimov IR. Optical mapping of the isolated coronary-perfused human sinus node. J Am Coll Cardiol. 2010; 56(17):1386–1394. [PubMed: 20946995]
28. Fedorov VV, Hucker WJ, Dobrzynski H, Rosenshtraukh LV, Efimov IR. Postganglionic nerve stimulation induces temporal inhibition of excitability in rabbit sinoatrial node. Am J Physiol Heart Circ Physiol. 2006; 291(2):H612–623. [PubMed: 16565321]
29. Fedorov VV, Schuessler RB, Hemphill M, Ambrosi CM, Chang R, Voloshina AS, Brown K, Hucker WJ, Efimov IR. Structural and functional evidence for discrete exit pathways that connect the canine sinoatrial node and atria. Circ Res. 2009; 104(7):915–923. [PubMed: 19246679]
30. Glukhov AV, Flagg TP, Fedorov VV, Efimov IR, Nichols CG. Differential K(ATP) channel pharmacology in intact mouse heart. J Mol Cell Cardiol. 2010; 48(1):152–160. doi:10.1016/j.yjmcc.2009.08.026. [PubMed: 19744493]
31. Greener ID, Tellez JO, Dobrzynski H, Yamamoto M, Graham GM, Billeter R, Boyett MR. Ion channel transcript expression at the rabbit atrioventricular conduction axis. Circ Arrhythm Electrophysiol. 2009; 2(3):305–315. [PubMed: 19808481]
32. Haberl R, Steinbeck G, Luderitz B. Comparison between intracellular and extracellular direct current recordings of sinus node activity for evaluation of sinoatrial conduction time. Circulation. 1984; 70(4):760–767. [PubMed: 6478574]
33. Hucker WJ, Fedorov VV, Foyil KV, Moazami N, Efimov IR. Images in cardiovascular medicine. Optical mapping of the human atrioventricular junction. Circulation. 2008; 117(11):1474–1477. [PubMed: 18347223]

34. Hucker WJ, McCain ML, Laughner JI, Iaizzo PA, Efimov IR. Connexin 43 expression delineates two discrete pathways in the human atrioventricular junction. Anat Rec (Hoboken). 2008; 291(2): 204–215. [PubMed: 18085635]
35. Hucker WJ, Nikolski VP, Efimov IR. Autonomic control and innervation of the atrioventricular junctional pacemaker. Heart Rhythm. 2007; 4(10):1326–1335. doi:10.1016/j.hrthm.2007.06.011. [PubMed: 17905339]
36. Inada S, Hancox JC, Zhang H, Boyett MR. One-dimensional mathematical model of the atrioventricular node including atrio-nodal, nodal, and nodal-his cells. Biophys J. 2009; 97(8): 2117–2127. [PubMed: 19843444]
37. Inoue S, Becker AE. Posterior extensions of the human compact atrioventricular node: a neglected anatomic feature of potential clinical significance. Circulation. 1998; 97(2):188–193. [PubMed: 9445172]
38. Irisawa H. Membrane currents in cardiac pacemaker tissue. Experientia. 1987; 43(11–12):1131–1135. [PubMed: 2446905]
39. James TN, Sherf L, Fine G, Morales AR. Comparative ultrastructure of the sinus node in man and dog. Circulation. 1966; 34(1):139–163. [PubMed: 5942665]
40. Juillard A, Guillerm F, Chuong HV, Barrillon A, Gerbaux A. Sinus node electrogram recording in 59 patients. Comparison with simultaneous estimation of sinoatrial conduction using premature atrial stimulation. Br Heart J. 1983; 50(1):75–84. [PubMed: 6860514]
41. Kerr CR, Prystowsky EN, Browning DJ, Strauss HC. Characterization of refractoriness in the sinus node of the rabbit. Circ Res. 1980; 47(5):742–756. [PubMed: 7418132]
42. Kirchhof CJ, Bonke FI, Allessie MA, Lammers WJ. The influence of the atrial myocardium on impulse formation in the rabbit sinus node. Pflugers Arch. 1987; 410(1–2):198–203. [PubMed: 3684505]
43. Kodama I, Boyett MR. Regional differences in the electrical activity of the rabbit sinus node. Pflugers Arch. 1985; 404(3):214–226. [PubMed: 4034368]
44. Kodama I, Nikmaram MR, Boyett MR, Suzuki R, Honjo H, Owen JM. Regional differences in the role of the Ca2+ and Na+ currents in pacemaker activity in the sinoatrial node. Am J Physiol. 1997; 272(6 Pt 2):H2793–2806. [PubMed: 9227559]
45. Kucera JP, Kleber AG, Rohr S. Slow conduction in cardiac tissue, II: effects of branching tissue geometry. Circ Res. 1998; 83(8):795–805. [PubMed: 9776726]
46. Lang D, Petrov V, Lou Q, Osipov G, Efimov IR. Spatiotemporal control of heart rate in a rabbit heart. J Electrocardiol. 2011; 44(6):626–634. [PubMed: 21937057]
47. Li J, Greener ID, Inada S, Nikolski VP, Yamamoto M, Hancox JC, Zhang H, Billeter R, Efimov IR, Dobrzynski H, Boyett MR. Computer three-dimensional reconstruction of the atrioventricular node. Circ Res. 2008; 102(8):975–985. [PubMed: 18309098]
48. Masson-Pevet MA, Bleeker WK, Besselsen E, Treytel BW, Jongsma HJ, Bouman LN. Pacemaker cell types in the rabbit sinus node: a correlative ultrastructural and electrophysiological study. J Mol Cell Cardiol. 1984; 16(1):53–63. [PubMed: 6699918]
49. Moe GK, Preston JB, Burlington H. Physiologic evidence for a dual A-V transmission system. Circ Res. 1956; 4(4):357–375. [PubMed: 13330177]
50. Nikolski VP, Jones SA, Lancaster MK, Boyett MR, Efimov IR. Cx43 and dual-pathway electrophysiology of the atrioventricular node and atrioventricular nodal reentry. Circ Res. 2003; 92(4):469–475. [PubMed: 12600895]
51. Opthof T. Function and structure of the mouse sinus node: nothing you can see that isn't shown. Cardiovasc Res. 2001; 52(1):1–4. [PubMed: 11557227]
52. Opthof T, de Jonge B, Masson-Pevet M, Jongsma HJ, Bouman LN. Functional and morphological organization of the cat sinoatrial node. J Mol Cell Cardiol. 1986; 18(10):1015–1031. [PubMed: 3783721]
53. Rohr S, Kucera JP, Fast VG, Kleber AG. Paradoxical improvement of impulse conduction in cardiac tissue by partial cellular uncoupling. Science. 1997; 275(5301):841–844. [PubMed: 9012353]

54. Roithinger FX, Cheng J, SippensGroenewegen A, Lee RJ, Saxon LA, Scheinman MM, Lesh MD. Use of electroanatomic mapping to delineate transseptal atrial conduction in humans. Circulation. 1999; 100(17):1791–1797. [PubMed: 10534466]
55. Saffitz JE, Kanter HL, Green KG, Tolley TK, Beyer EC. Tissue-specific determinants of anisotropic conduction velocity in canine atrial and ventricular myocardium. Circ Res. 1994; 74(6):1065–1070. [PubMed: 8187276]
56. Sherf L, James TN, Woods WT. Function of the atrioventricular node considered on the basis of observed histology and fine structure. J Am Coll Cardiol. 1985; 5(3):770–780. [PubMed: 3973277]
57. Shibata N, Inada S, Mitsui K, Honjo H, Yamamoto M, Niwa R, Boyett MR, Kodama I. Pacemaker shift in the rabbit sinoatrial node in response to vagal nerve stimulation. Exp Physiol. 2001; 86(2): 177–184. [PubMed: 11429632]
58. Spach MS, Miller WT 3rd, Geselowitz DB, Barr RC, Kootsey JM, Johnson EA. The discontinuous nature of propagation in normal canine cardiac muscle. Evidence for recurrent discontinuities of intracellular resistance that affect the membrane currents. Circ Res. 1981; 48(1):39–54. [PubMed: 7438345]
59. Vassall-Adams PR. Ultrastructure of the human atrioventricular conduction tissues. Eur Heart J. 1983; 4(7):449–460. [PubMed: 6628421]
60. Verheijck EE, Wessels A, van Ginneken AC, Bourier J, Markman MW, Vermeulen JL, de Bakker JM, Lamers WH, Opthof T, Bouman LN. Distribution of atrial and nodal cells within the rabbit sinoatrial node: models of sinoatrial transition. Circulation. 1998; 97(16):1623–1631. [PubMed: 9593568]
61. Vetter FJ, McCulloch AD. Three-dimensional analysis of regional cardiac function: a model of rabbit ventricular anatomy. Prog Biophys Mol Biol. 1998; 69(2–3):157–183. [PubMed: 9785937]
62. Wang K, Ho SY, Gibson DG, Anderson RH. Architecture of atrial musculature in humans. Br Heart J. 1995; 73(6):559–565. [PubMed: 7626357]
63. Woods WT, Sherf L, James TN. Structure and function of specific regions in the canine atrioventricular node. Am J Physiol. 1982; 243(1):H41–50. [PubMed: 7091378]
64. Wu J, Wu J, Olgin J, Miller JM, Zipes DP. Mechanisms underlying the reentrant circuit of atrioventricular nodal reentrant tachycardia in isolated canine atrioventricular nodal preparation using optical mapping. Circ Res. 2001; 88(11):1189–1195. [PubMed: 11397786]
65. Yamamoto M, Honjo H, Niwa R, Kodama I. Low-frequency extracellular potentials recorded from the sinoatrial node. Cardiovasc Res. 1998; 39(2):360–372. [PubMed: 9798521]
66. Zhang H, Holden AV, Boyett MR. Gradient model versus mosaic model of the sinoatrial node. Circulation. 2001; 103(4):584–588. [PubMed: 11157726]
67. Zhang H, Holden AV, Kodama I, Honjo H, Lei M, Takagishi Y, Boyett MR. Hypothesis to explain the block zone protecting the sinoatrial node. Biophysics Journal. 1999; 76:A368–A368.
68. Zhang H, Holden AV, Kodama I, Honjo H, Lei M, Varghese T, Boyett MR. Mathematical models of action potentials in the periphery and center of the rabbit sinoatrial node. Am J Physiol Heart Circ Physiol. 2000; 279(1):H397–421. [PubMed: 10899081]

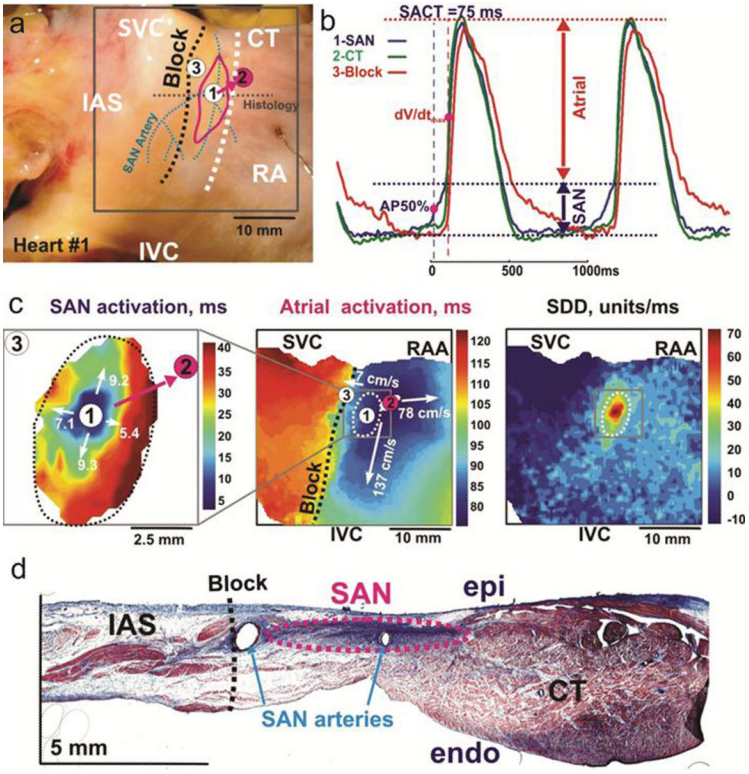

Fig. 1.

a Epicardial aspect of a perfused SAN preparation. The three dashed lines are: black for block zone, white for sulcus terminalis, blue for SAN arteries. The solid pink line demarcates the location of the SAN. The solid circles are atrial exit breakthrough points recorded in all preparations, the pink circle is the intrinsic breakthrough point of this preparation **b** Optical APs from SAN (blue), breakthrough point in CT (green) and block zone (red) during intrinsic sinus rhythm (cycle length 1070ms). Several components to the APs reflect superimposed signals from overlying areas. The SAN component is smaller than the atrial one **c** Separate activation maps of the SAN and right atrium allow tracking of the exit pathway. Also shown here a slow diastolic depolarization (SDD) map of the right atrium **d** Histological section through the SAN demonstrating surrounding connective tissue layers and presence of arterial branches at the block zone. AP50%: 50% of SAN AP amplitude, dV/dt_{max}: maximum derivative of atrial upstroke, IVC: inferior vena cava, SVC: superior vena cava, RAA: right atrial appendage, epi: epicardium, endo: endocardium (Reproduced from Fedorov et al. [27] with permission).

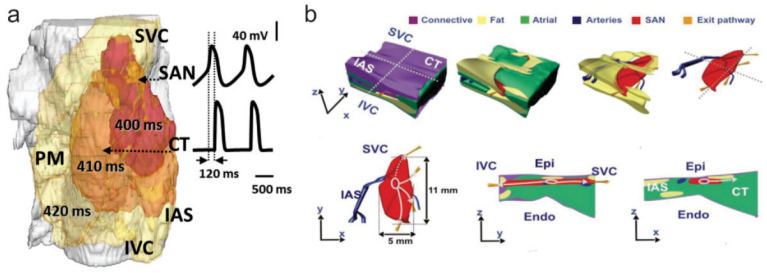

Fig. 2.

a Activation sequence simulated with the 3D human SAN model by Chandler et al. Snapshots of membrane potential isosurface V=−30 mV in the semi-transparent tissue are shown at 400, 410 and 420 ms, along with time courses of the membrane potential in the SAN and CT. Conduction time between the earliest excitation in the SAN and the earliest atrial activation in the CT is ~120 ms, after which the excitation rapidly spreads through the atrial tissue **b** Anatomical model of the human SAN based on histological reconstruction and incorporating functional sino-atrial exit pathways (gold), shown in different projections. Surrounding tissues are: connective tissue (purple), fat (yellow), atrial muscle (green) and arteries (blue). SAN: sinoatrial node, CT: crista terminalis, PM: pectinate muscles, IAS: inter-atrial septum, SVC: superior vena cava, IVC: inferior vena cava, Epi: epicardium, Endo: endocardium (Fig. 2b reproduced from Fedorov et al. [27] with permission)

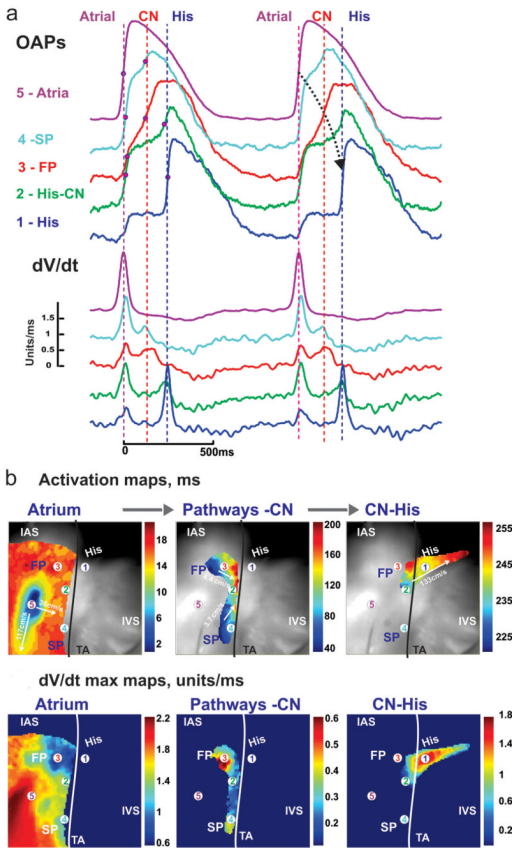

Fig. 3.

a Optical APs and their maximum derivatives from five recording sites in the human AVN preparation during atrial pacing at cycle length 1000ms (recording sites are solid circles in **b** and **c**, superimposed on the optical field of view, which is 30×30 mm^2) **b** Separate activation maps of the right atrium, AVN and His bundle allow tracking of conduction with conduction velocities. Black line represents the tricuspid valve annulus **c** dV/dt_{max} maps in the same areas. FP: fast pathway, SL: slow pathway, IAS: inter-atrial septum, IVS: inter-ventricular septum, CN: compact node (Reproduced from Fedorov et al. [25] with permission)